Cancer Management and Research

Dovepress

open access to scientific and medical research

Open Access Full Text Article

ORIGINAL RESEARCH

Exosome-Encapsulated MicroRNA-21 from Esophageal Squamous Cell Carcinoma Cells Enhances Angiogenesis of Human Umbilical Venous Endothelial Cells by Targeting SPRY1

This article was published in the following Dove Press journal:
Cancer Management and Research

Huirong Zhuang[1]
Hongjun Wang[2]
Haibo Yang[2]
Hongli Li[1]

[1]Operating Room, East Medical District of Linyi People's Hospital, Linyi 276034, People's Republic of China; [2]Department of Occupational Disease, Linyi People's Hospital, Linyi 276000, People's Republic of China

Objective: Esophageal squamous cell carcinoma (ESCC) persists among the most prevalent cancers worldwide. Angiogenesis represents a crucial element necessitated for tumor growth and metastasis in ESCC. In this study, we aimed to study the effect of microRNA (miR)-21 on angiogenesis in ESCC and its underlying mechanism.

Materials and Methods: Initially, the expression patterns of miR-21, SPRY1, and VEGF were determined in ESCC tissues and cells. The relationship between miR-21 and SPRY1 was identified using dual-luciferase reporter assay. Exosomes were subsequently isolated from the ESCC cells, followed by co-culture with the human umbilical venous endothelial cells (HUVECs). HUVEC proliferation and angiogenesis were determined by means of CCK-8, colony formation, and microtubule formation in vitro. Chicken chorioallantoic membrane (CAM) model and mouse xenograft model of ESCC cells were established to substantiate the function of miR-21 corresponding to the angiogenesis and tumor growth of ESCC, followed by microvascular density (MVD) evaluation.

Results: Expression patterns of miR-21 and VEGF were elevated, while the SPRY1 expression pattern was repressed in ESCC tissues and cells. The downregulation of miR-21 and exosome-derived miR-21 impeded the proliferation and angiogenesis in HUVECs. Our data revealed that miR-21 could negatively target SPRY1, and positively target VEGF. The downregulation of miR-21 could evidently encumber the angiogenesis and tumor growth of ESCC in vivo, as evidenced by the decrease in number of branches of the microvessels and MVD.

Conclusion: Collectively, ESCC cell-derived exosome containing miR-21 promotes the proliferation and angiogenesis of HUVECs via SPRY1 downregulation and VEGF upregulation.

Keywords: esophageal squamous cell carcinoma, angiogenesis, exosomes, microRNA-21, Sprouty RTK signaling antagonist 1, vascular endothelial growth factor

Correspondence: Hongli Li
Operating Room, East Medical District of Linyi People's Hospital, No. 233, Fenghuang Street, Hedong District, Linyi, Shandong Province 276034, People's Republic of China
Tel +86-539-8096762
Email Lihongliddtc8@163.com

Introduction

Esophageal cancer has emerged as an alarming public health concern, ranking as the 7th most prevalent cancer with 572,000 new cases annually and over 500,000 deaths in 2018.[1] Esophageal squamous cell carcinoma (ESCC) as the dominant subtype accounts for approximately 90% of esophageal cancer cases worldwide.[2,3] The principal ESCC etiological factors include smoking and alcohol, with a higher cancer predisposition

submit your manuscript | www.dovepress.com
DovePress
http://doi.org/10.2147/CMAR.S259077

among males.[4] Peculiar angiogenesis is an invasive indicator of tumor growth and metastasis in several diseases.[5,6] ESCC has also been reported to initiate angiogenesis, highlighting the potential of inhibiting tumor angiogenesis as a therapeutic approach for the treatment of ESCC.[7]

Exosomes have been regarded as nano-sized bio-vesicles, which are released into surrounding body fluids upon fusion of multivesicular bodies with the plasma membrane.[8,9] Exosomes could efficaciously transfer several biological compounds such as mRNAs, microRNAs (miRNAs), proteins and lipids to the targeted cells.[10] An existing study documented the elicited the functionality of circulating microRNAs (miRNAs or miRs) as potential diagnostic markers for gastric and esophageal cancers.[11] Exosome-encapsulated miRNAs could evidently exercise pivotal functions in a variety of cancers including ovarian cancer[12] and gastric cancer[13] by radically initiating angiogenesis. Intriguingly, the differentially expressed miRs are contained in exosomes derived from ESCC cells under hypoxic conditions.[14] Additionally, miR-21 has been implicated in the development and progression of various cancers, with studies highlighting its potential as a biomarker for cancer diagnosis and prognosis.[15] An existing study elicited the potential of miR-21 as a biomarker for ESCC. Interestingly, the involvement of exosome-encapsulated miR-21 in the development and progression of ESCC has demonstrated miR-21 as a viable clinical biomarker.[17] Moreover, research has cited an association between exosome-derived miR-21 and enhanced angiogenesis of lung cancer.[18] The regulatory role of miR-21 in sprouty RTK signaling antagonist 1 (SPRY1) has been investigated as a therapeutic modality for neovascularization.[19] SPRY1 fundamentally functions as an inhibitor of the Ras-mitogen-activated protein kinase (MAPK) signaling pathway.[20] Upregulated expression of SPRY1 in the human umbilical venous endothelial cell (HUVEC) can efficaciously inhibit angiogenesis via upregulation of p21 and p27.[21] Compelling evidence has demonstrated the vitality of vascular endothelial growth factor (VEGF) in abnormal angiogenesis to substantiate VEGF as a key target in anti-angiogenic therapy.[22] VEGF is involved in various vascularization processes[23] with significant functionality in the ESCC angiogenesis process.[24] Interestingly, a close relationship between miR-21 and VEGF has been identified in hepatocellular carcinoma.[25] On the basis of the microarray and experimental analyses, we hypothesized that exosome-encapsulated miR-21 derived from ESCC cells regulates SPRY1-dependent VEGF, ultimately manipulating the proliferation, and angiogenesis in HUVECs. Hence, an ESCC cell line was chosen, followed by establishment of a chicken chorioallantoic membrane (CAM) model and a mouse model to investigate the potential regulatory mechanism of exosome-derived miR-21 in ESCC.

Materials and Methods

Ethics Statement

The current study was performed with approval of the Ethics Committee of Linyi People's Hospital and in strict accordance with the *Declaration of Helsinki* issued in 1975. All participants provided signed informed consent prior to enrollment. All animal experiments were conducted with the approval of the Ethics Committee of Linyi People's Hospital and in strict accordance with the guidelines issued in the Guide for the Care and Use of Laboratory Animals published by the US National Institutes of Health. Adequate efforts were taken to ensure minimal animal suffering during the study.

Microarray-Based Gene Expression Profiling

The ESCC-related miR expression dataset (GSE97049) and 2 gene expression datasets (GSE45670 and GSE29001) were retrieved from the Gene Expression Omnibus (GEO) database (https://www.ncbi.nlm.nih.gov/geo/), followed by a differential expression analysis (Table 1). The R language affy package (http://www.bioconductor.org/packages/release/bioc/html/affy.html) was adopted for background correction and the standardized preprocessing of the expression data, followed by differential expression analysis using the limma package (http://master.bioconductor.org/packages/release/bioc/html/limma.html). The heatmap was subsequently plotted based on the provided data using the heatmap package (https://cran.r-project.org/web/packages/pheatmap/index.html). The potential target genes of the differentially expressed miRs were predicted using a combination of the miRDB (http://www.mirdb.org/), DIANA (http://diana.imis.athena-innovation.gr/DianaTools/index.php?r=microT_CDS/index), and TargetScan websites (http://www.targetscan.org/vert_71/). Finally, the differentially expressed genes (DEGs) exhibiting a target relationship with the differentially expressed miRs were screened using the JVenn (http://jvenn.toulouse.inra.fr/app/example.html).

Sample Collection

Human normal esophageal epithelial cell line (Het-1A) and human ESCC cell lines (EC9706, Eca109, KYSE-150, TE-1,

Table 1 Gene and miR Expression Datasets Retrieved from the GEO Database

Accession	Platform	Type	Organism	Sample
GSE97049	GPL21572	miR	Homo sapiens	7 esophageal squamous cell carcinoma tissues and 7 adjacent normal tissues
GSE45670	GPL570	Gene	Homo sapiens	28 esophageal squamous cell carcinomas and 10 normal esophageal epithelia
GSE29001	GPL571	Gene	Homo sapiens	21 esophageal squamous cell carcinoma tumor and 24 match normal

Notes: miR, microRNA; GEO, Gene Expression Omnibus.

and TE-5) acquired from the American Type Culture Collection (ATCC; Manassas, VA, USA) were passaged within 6 months. All cell lines were detected by mycoplasma and short-tandem-repeat (STR). The cells were cultured in a 5% CO_2 incubator at 37°C in the Roswell Park Memorial Institute (RPMI)-1640 medium containing 10% fetal bovine serum (FBS), 100 μg/mL streptomycin, and 100 U/mL penicillin.

A total of 113 pairs of ESCC and matched adjacent normal tissue samples were harvested from ESCC patients (85 males and 28 females) that underwent surgical treatment via thoracic surgical resection at Linyi People's Hospital between a period ranging from April 2015 and November 2018. All participants were pathologically confirmed as ESCC post-operation. The exclusion criteria for the patients were as follows: patients with trache-esophageal fistula or incomplete esophageal obstruction, normal hemogram and adequate function of major organs (including cardiac, hepatic, and renal function). Ineligibility criteria were as follows: an active uncontrolled infection, clinically significant cardiovascular disease, history of past malignancies, and previous therapeutic intervention with radiotherapy, chemotherapy or immunotherapy. Furthermore, according to the 8th edition of the American Joint Committee on Cancer (AJCC) tumor-node-metastasis (TNM) system, the patients were classified as 7 cases in stage IA, 4 cases in stage IB, 21 cases in stage IIA, 29 cases in stage IIB, 52 cases in stage III.[26] Among the patients, there were 49 cases <61 years old and 64 cases ≥61 years old with a median age of 62 years old. The patients consisted of all degree of ESCC ranging from poorly (27 cases), moderately (53 cases) and highly (33 cases) differentiated ESCC.

Immunohistochemistry

ECSS and the adjacent normal tissues were dewaxed, followed by a rinse for antigen retrieval. After a blockade with 3% formaldehyde to eliminate any peroxidase activity, the goat serum blocking solution containing the primary antibody to VEGF (Sc-7269, 1: 100, Santa Cruz, CA, USA) as well as the secondary antibody peroxide-labeled streptavidin working solution was added to the tissues sequentially. Diaminobenzidine (DAB) was subsequently added for color development, followed by hematoxylin counterstaining, dehydration, permeabilization, and mounting. Finally, a total of five fields were randomly selected from each section, after which the positive expression was evaluated based on an existing literature.[27]

Cell Treatment

ESCC cell line KYSE-150 was cultured using the RPMI-1640 medium (Gibco, Carlsbad, CA, USA) supplemented with bovine exosomes containing 10% FBS, 100 μg/mL streptomycin, and 100 U/mL penicillin, followed by culture in a 5% CO_2 incubator under saturated humidity at 37°C. The medium was replaced every 2–3 days. Upon attaining 80%-90% cell confluence, the cells were treated with 0.25% trypsin (Gibco) supplemented with 0.02% ethylenediaminetetraacetic acid and passaged at a ratio of 1: 2–3. Next, 30 mL of the complete medium and cells (1×10^8 cells/mL) were added into a 175 cm^2 cell culture flask and cultured for 48 h. The cell supernatant in the logarithmic phase was then collected.

Prior to transfection, KYSE-150 cells in the logarithmic phase were digested and then seeded in cell culture plates at a density of 3×10^5 cells/well.[28] The cells were infected with several lentiviruses containing agomir-negative control (NC), miR-21 agomir, antagomir-NC, miR-21 antagomir or miR-21 agomir + oe-SPRY1 using Lipofectamine™ RNAiMAX (Invitrogen, Carlsbad, CA, USA).

Isolation and Characterization of Exosomes Derived from ESCC Cells

The supernatant was collected after centrifugation (300 × g, 10 min; 1200 × g, 20 min; 100,000 × g, 30 min), while the precipitate was collected after centrifugation at 100,000

g and 4°C. The precipitate was rinsed, resuspended using clean phosphate-buffered saline (PBS), and then centrifuged at 100,000 g and 4°C for 2 h. The exosomes were resuspended using 100 μL of PBS and preserved at −80°C.

The exosome suspension (20 μL) was placed on a copper grid for 1 min at room temperature, and then combined with 10 μL of the phosphotungstic acid solution (1%; Jiuding Chemical Technology Co., Ltd., Shanghai, China), followed by counterstaining for 1 min at room temperature. The exosome suspension was then dried with an incandescent lamp and then observed under a transmission electron microscope (TEM).

The exosome precipitates obtained by centrifugation were subsequently dissolved in 500 μL PBS to prepare the suspension, which was then diluted at a ratio of 1:100. Next, 300 μL of the supernatant was collected, and stored at 20°C, followed by analysis of the particle size using the Nanosight LM10-HS nanoparticle analyzer (Malvern, UK).

The exosome suspension was concentrated, after which the protein content was determined using a bicinchoninic acid (BCA) kit (23227, Thermo Fisher, Austin, Texas, USA). The protein was then subjected to sodium dodecyl sulfate polyacrylamide gel electrophoresis (SDS-PAGE) and transferred onto the membrane. Immunoblotting was then conducted to detect the protein levels of the exosome-specific markers tumor susceptibility gene 101 (TSG101) (ab30871), CD63 (ab216130), CD81 (ab109201), and GRP94 (ab13509) (all Abcam, Cambridge, UK).

Co-Culture of Exosomes and HUVECs

The exosomes were mixed with exo-Red (EXOR100A-1; Changzhou Byxbio, Jiangsu, China) at a volume ratio of 10:1.[29] The mixture was then incubated at 37°C for 10 min, terminated by the addition of 100 μL of the stop solution, followed by an additional incubation at 4°C for 30 min. The supernatant was then centrifuged. Next, the fluorescent-labeled exosomes were resuspended using 200 μL of PBS. Upon attaining 50–60% cell confluence, the HUVEC supernatants were seeded onto 24-well plates and then incubated with the fluorescent-labeled exosomes (exosomes from ESCC cells infected with PBS, agomir-NC or miR-21 agomir, respectively) for 48 h. An inverted microscope was then used to analyze the HUVECs, followed by application of reverse transcription quantitative polymerase chain reaction (RT-qPCR) to determine the expression pattern of miR-21.

Dual Luciferase Reporter Assay

The target genes of miR-21 were predicted in accordance with the bioinformatic website (https://cm.jefferson.edu/rna22/Interactive/), and the relationship between SPRY1 and miR-21 was subsequently validated by dual-luciferase reporter assay. KYSE-150 cells were cultured in 24-well plates, and transduced with agomir-NC, miR-21 agomir and wild type (WT)-miR-21/SPRY1 or mutant (MUT)-miR-21/SPRY1. The cells were harvested following a regimen of 48-h transfection. After centrifugation of the cell lysate, 40 μL of firefly luciferase and firefly luciferin was added to each tube, with measurement of the fluorescence intensity promptly 10 s after mixing. The value of Firefly luciferase activity/Renilla luciferase activity was normalized.

RNA Extraction and Quantification

The total RNA content extracted from cells or tissues was reversely transcribed into complementary DNA (cDNA) in strict accordance with the provided instructions of the reverse transcription kit. The primer sequences are listed in Table 2. RT-qPCR was subsequently performed in strict accordance with the provided instructions of the Applied Biosystems kit (Thermo Fisher) on an ABI 7500 instrument (Applied Biosystems, Foster City, CA, USA). U6 (for miR-21) where glyceraldehyde-3-phosphate dehydrogenase (GAPDH) (for the remaining genes) was regarded as an internal reference, and the fold changes were subsequently calculated based on relative quantification ($2^{-\Delta Ct}$ method).

Immunoblotting

The total protein content was extracted from the ESCC cells or tissues using a radio-immunoprecipitation assay lysis buffer (Beyotime Biotechnology, Shanghai, China). The extracted proteins were separated using 10% SDS-PAGE and subsequently transferred onto a nitrocellulose membrane, which underwent a blockade using skim milk powder (3%) at room temperature for 1 h. The membrane was probed overnight at 4°C with the primary antibodies, and re-probed with the secondary antibody horseradish peroxidase-labeled immunoglobulin G (IgG) (ab109489, 1:1000, Abcam). After 2 rinses with the Tris-buffered saline Tween-20 (TBST), the membrane was visualized using the enhanced chemiluminescence reagent (Santa Cruz Biotechnology, Inc, Santa Cruz, CA, USA), with the band intensities analyzed by the ImageJ1.48u software. The included primary antibodies

Table 2 Primer Sequences for RT-qPCR

Gene of Interest	Primer Sequence (5′-3′)	
miR-21	F: GCCCGCTAGCTTATCAGACTGATG	R: GTGCAGGGTCCGAGGT
SPRY1	F: GCAGTGGCAGTTCGTTAGTTG	R: CAGTAGGCTGAATCTCTCTCTCA
VEGF	F: CAAACGCTGACATGTACGGTCTA	R: CCAACTGCCAATACCAGTGGAT
U6	F: CGCTTCGGCAGCACATATACTA	R: CGCTTCACGAATTTGCGTGTCA
GAPDH	F: TCACCCACACTGTGCCCATCTACGA	R: CAGCGGAACCGCTCATTGCCAATGG

Abbreviations: RT-qPCR, reverse transcription quantitative polymerase chain reaction; miR-21, microRNA-21; SPRY1, Sprouty RTK signaling antagonist 1; GAPDH, glyceraldehyde-3-phosphate dehydrogenase; U6, small nuclear RNA; F, forward; R, reverse.

were as follows: rabbit anti-human SPRY1 (ab75492, 1:1000), rabbit anti-human VEGF (sc-7269, 1:500; Santa Cruz), GAPDH (ab8245, 1:1000, Abcam), and anti-β-actin antibody (ab8227, 1:5000, Abcam).

Enzyme-Linked Immunosorbent Assay (ELISA)

The medium of the co-cultured cells was collected after evaluating the VEGF content based on the provided instructions of the ELISA kit (Immunotech International, Marseille, France). The optical density (OD) values of each well were measured at an excitation wavelength of 490 nm using a microplate reader (BIO-RAD Laboratories, Hercules, CA, USA). The OD value of samples/OD value of NC > 1.5 was considered to be positive.

Microtubule Formation in Vitro

HUVECs (5×10^3 cells/well) were seeded into 96-well plates and cultured for 18 h at 37°C in strict accordance with the provided instructions of the in vitro angiogenesis assay kit (Amulet scientific, BioVision, San Francisco, US). Tube formation was subsequently observed under an inverted microscope (IX73; Olympus Optical Co., Ltd., Tokyo, Japan) before counting the number of blood vessel forming nodes per well from 10 randomly selected fields, after which the average values were calculated.

Colony Formation Assay

HUVECs obtained from ATCC (PCS-100-010) were prepared into a single cell suspension, and then seeded into a 60 mm dish (1000 cells/60 mm), followed by culture in CO_2. The culture medium was replaced every 3 days. Fourteen days later, the HUVECs were fixed using formaldehyde for 15 min and stained with crystal violet for 15 min. The number of colonies (cell colonies >50) was counted under an inverted microscope (CKX31; Olympus Optical Co., Ltd.). Colony formation rate was calculated as the number of colonies/the number of HUVECs seeded × 100%.

Cell Counting Kit-8 (CCK-8) Assay

The viability of the HUVECs was assessed using the CCK-8 kit (MAO218, Meilun Biotechnology® Company, Dalian, China). Briefly, the cells were prepared into a single suspension and then seeded into a 96-well plate. Next, 10% CCK-8 reagent was added to the cells at 1, 2, 3, 4, and 5 days, respectively, followed by a 2-hour regimen of incubation at 37°C, with five replicate wells set. The OD value was measured at an excitation wavelength of 450 nm using a microplate reader (Stat Fax 2100; Awareness, USA).

Establishment of CAM Models of the Chicken Embryo

A total of 50 fertilized Nick Chick white eggs weighing 50–55 g were acquired from Jinan Sparfas Poultry Co., Ltd. (Jinan, Shandong, China) and incubated at 37°C with 40–60% humidity. The eggs were turned twice per day, with exclusion of stillbirth or developmental dysplasia of embryo. KYSE-150 cells were suspended in serum-free medium, and then supplemented with an equal volume of Matrigel (BD Biosciences, Bedford, MA, USA). The mixture was instilled into CAM incubated on the 9th day (10 eggs/group) with a success rate of 80%. The branching of surrounding blood vessels around the 5 mm area in the implanted Matrigel was counted 4 days after implantation.

Tumor Xenografts in Nude Mice

A total of 32 specific pathogen-free (SPF) BALB/c female nude mice, weighing 16–20 g and aging 4–6 weeks were acquired from the Hunan SJA Laboratory Animal Co., Ltd. (Changsha, Hunan, China). The mice were placed on a meticulous diet for 7 days prior to experimentation. The KYSE-150 cells were transduced with the agomir-NC, miR-21 agomir, antagomir-NC, or miR-21 antagomir, and then

prepared into a single cell suspension (1×10^7 cells/mL). The single cell suspension (0.2 mL; twice every week) was subcutaneously injected into the right forelimbs of the nude mice. Tumor length (L) and width (S) were measured every 7 days 2nd week onwards, and the tumor volume (V) was calculated according to the formula ($V = 0.5 \times L \times S^2$). A growth curve of the transplanted tumor was subsequently plotted. Following a 28-day period of observation, the nude mice were euthanized and estimation of the wet weight of the tumor, followed by calculation of the tumor inhibition rate. The tumor tissues of nude mice were fixed with 10% formaldehyde, paraffin-sectioned, and conclusively subjected to microvascular density (MVD) evaluation.

MVD Evaluation

Labeled streptavidin biotin (LSAB) kit (Dako, SouthSan Francisco, California, USA) was employed to evaluate MVD with PBS in lieu of the primary antibody serving as NC. The positive control was provided by Vector (Silicon Valley, CA, USA). The tumor tissue sections were incubated with 0.5% H_2O_2 for 15 min at room temperature and further incubated with the horse serum (1:80) for another 20 min. The sections were then probed with the DBA-diluted mouse anti-human FVIII-Ag (1:150; Vector) at room temperature for 60 min and then re-probed with the secondary antibody (1:200) or freshly prepared ABC for 60 min at room temperature, respectively. DAB and 0.5% H_2O_2 were applied prior to incubation for 10 min before counterstaining the sections with hematoxylin for 15 s. MVD was determined based on the Weidner protocol.[30] The microvessels were counted under 3 visual fields with the average number defined as the MVD of the tumor.

Statistical Analysis

All data were processed and analyzed using the SPSS 21.0 statistical software (IBM Corp., Armonk, New York, USA). Measurement data were expressed as mean ± standard deviation from three independent experiments. The paired *t*-test was employed for comparisons between ESCC and the adjacent normal tissues while the unpaired *t*-test was employed for analysis of the unpaired data comparisons. Comparisons among multiple groups were conducted by means of one-way analysis of variance (ANOVA), followed by the Tukey's post hoc test with corrections for multiple comparisons. Statistical analysis of the time-based measurements within each group was performed using repeated measures ANOVA, followed by application of Bonferroni's post hoc test with corrections for multiple comparisons. In all statistical figures, a value of $p < 0.05$ was indicative of statistical significance.

Results

miR-21 Might Regulate Tumor Angiogenesis by Targeting SPRY1: Based on Microarray Analysis

The top 10 differentially expressed miRs were screened from the ESCC-related gene expression dataset GSE97049, on account of which a heatmap was plotted (Figure 1A). On the basis of the sequentially adjusted *p*-value, hsa-miR-21-5p was identified as the most significantly differentially expressed miR in ESCC, with a markedly high expression pattern in ESCC tissues than the adjacent normal tissues. The target genes of miR-21 were predicted using a combination of miRDB, DIANA, and TargetScan. Additionally, 62 genes were identified in miRDB by setting the Target Score >80, 108 genes were predicted in DIANA based on the miTG score >0.9, and 69 genes were predicted using TargetScan with a total context++ score <−0.4. The DEGs were screened from the ESCC-related gene expression datasets GSE45670 and GSE29001, with the results revealing 1510 downregulated DEGs in GSE45670, and 894 downregulated DEGs in GSE29001. In order to screen the DEGs that potentially regulated by miR-21, we intersected the genes in miRDB, DIANA, and TargetScan and DEGs from datasets GSE45670 and GSE29001, with retrieval of SPRY1 (Figure 1B).

The expression patterns of the top 20 DEGs in the gene expression dataset GSE45670 are illustrated in Figure 1C, with the expression pattern of SPRY1 in gene expression dataset GSE29001 depicted in Figure 1D, both of which indicated that SPRY1 was poorly expressed in ESCC. An existing study proposed that SPRY1 could inhibit angiogenesis,[21] while another study also evidenced that miR-21 could induce angiogenesis.[31] In addition, a study reported that miR-21 was secreted by the serum exosomes of patients with ESCC.[17] Thus, based on the microarray analysis and published literatures, we speculated that exosome-encapsulated miR-21 derived from ESCC cells could essentially regulate the tumor angiogenesis by targeting SPRY1.

miR-21 and VEGF are Highly Expressed, but SPRY1 is Poorly Expressed in ESCC Tissues

RT-qPCR was employed to determine the expression patterns of SPRY1, miR-21, and VEGF in the ESCC tissues

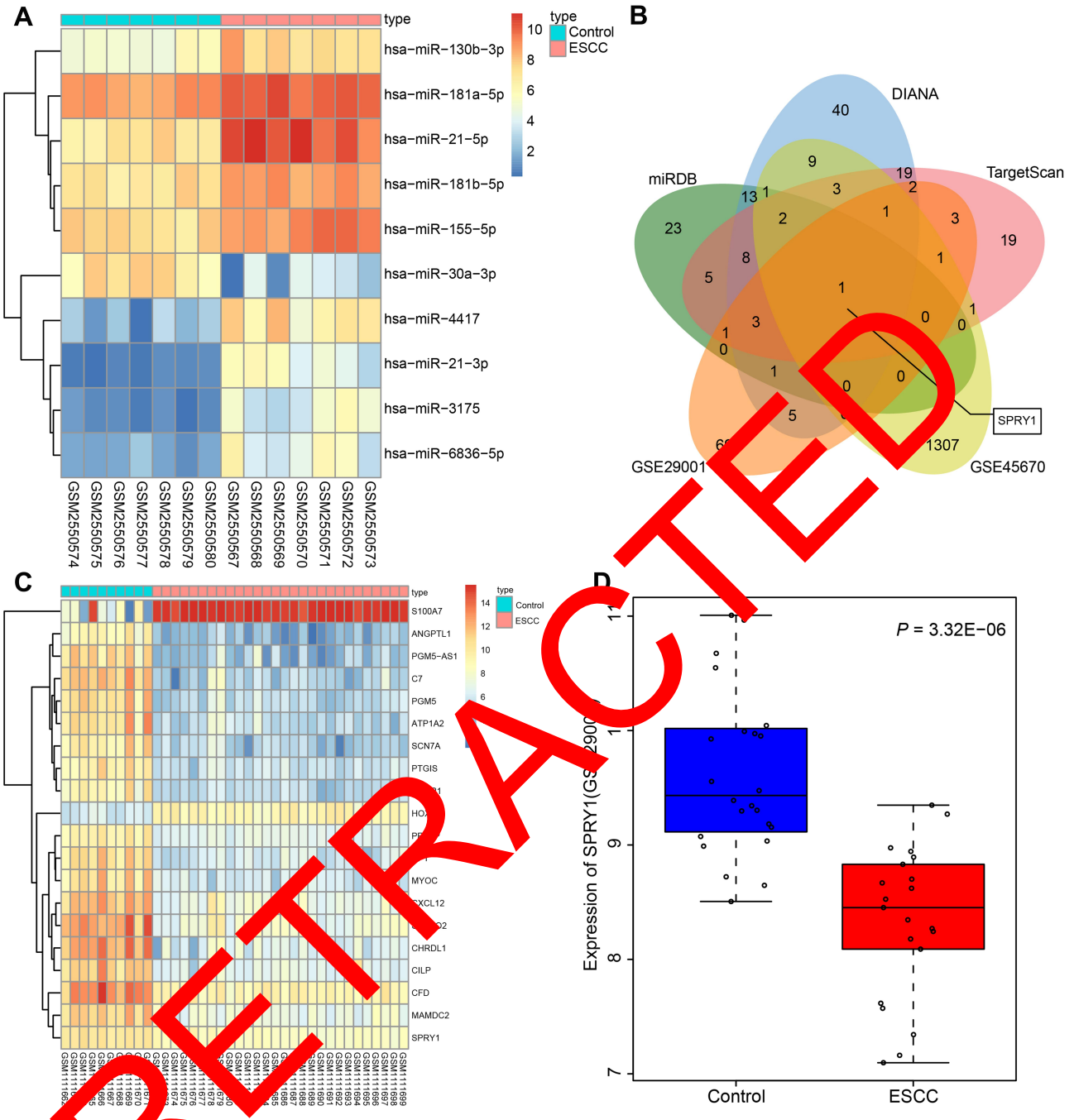

Figure 1 M...arr... based gene ...xpression profiling of DEGs and differentially expressed miRs in ESCC. (**A**) The heat map of the top 10 differentially expressed miRs obtained from t... ESCC-related gene expression dataset GSE97049. The x-axis represents the sample number, while the y-axis represents the differential miRNA. The right upper histogram re...sents the color gradation. Each rectangle in the figure corresponds to the expression of one sample. (**B**) The intersected genes of the targeted genes obtained from the mi... DIANA, and TargetScan databases, and DEGs from datasets GSE45670 and GSE29001. (**C**) The heatmap of top 20 DEGs predicted in the gene expression dataset GSE45670. The x-axis represents the sample number, while the y-axis indicates the DEGs. The histogram in the upper right represents the color gradation. Each rectangle in the figure corresponds to the expression of one sample. (**D**) The expression pattern of SPRY1 predicted in the gene expression dataset GSE29001.

and adjacent normal tissues, which demonstrated that miR-21 and VEGF were highly expressed, whereas SPRY1 was poorly expressed in the ESCC tissues compared to the adjacent normal tissues ($p < 0.05$) (Figure 2A). Immunohistochemistry was conducted to assess the positive expression pattern of VEGF protein in the ESCC tissues. The results revealed that VEGF positive expression pattern was predominately localized in the cytoplasm of ESCC tissues discernible by a brownish yellow color (Figure 2B). The positive rate of VEGF was notably

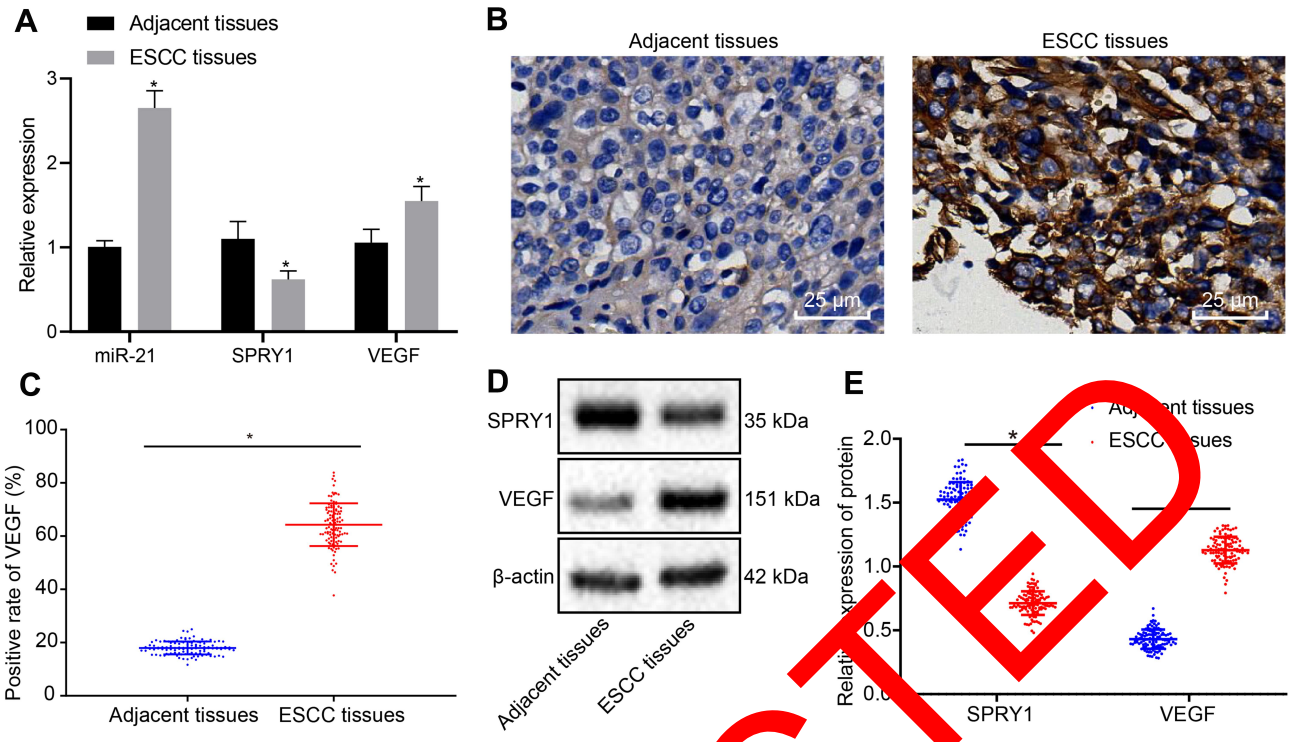

Figure 2 The expression patterns of miR-21 and VEGF are upregulated, but the SPRY1 expression pattern is downregulated in ESCC tissues compared to the adjacent normal tissues. (**A**) The expression patterns of miR-21, VEGF, and SPRY1 in the ESCC and adjacent normal tissues assessed using RT-qPCR. *$p < 0.05$ *vs* adjacent normal tissues (n = 113). (**B, C**) The positive expression pattern of VEGF protein in ESCC and adjacent normal tissues assessed using immunohistochemistry (400 ×, scale bar = 25 μm). (**D, E**) The protein expression patterns of VEGF and SPRY1 in the ESCC and adjacent normal tissues assessed using immunoblotting (SPRY1: 35 kDa, VEGF: 151 kDa). Paired *t*-test was conducted to analyze the data between the ESCC tissues and adjacent normal tissues (n = 113).

elevated in the ESCC tissues compared to the adjacent normal tissues (Figure 2C).

Next, the protein expression patterns of VEGF and SPRY1 were assessed by means of immunoblotting, the results of which identified an elevated VEGF expression pattern along with repressed expression pattern of SPRY1 in the ESCC tissues compared to the adjacent normal tissues ($p < 0.05$) (Figure 2D and E). Conjointly, the expression patterns of miR-21 and VEGF were elevated, while the SPRY1 expression pattern was downregulated in the ESCC tissues.

miR-21 Targets and Inhibits SPRY1 Expression

A specific binding site between SPRY1 and miR-21 was predicted via online analysis (Figure 3A), which was subsequently validated by dual luciferase reporter assay. The results displayed that the luciferase activity of SPRY1-WT was markedly diminished in response to miR-21 agomir compared to agomir-NC ($p < 0.05$), while no significant difference was evident in the luciferase activity of the SPRY1-MUT ($p > 0.05$) (Figure 3B), indicating that miR-21 could specifically bind to SPRY1.

For a comprehensive understanding of the function of miR-21 in the ESCC cells, we assessed the expression pattern of miR-21 in the human normal esophageal epithelial cell line (Het-1A) and human ESCC cell lines (Eca109, EC9706, TE-1, KYSE-150, and TE-5) using RT-qPCR. The results of which revealed that miR-21 was highly expressed in the ESCC cells compared to the Het-1A cells, with the highest expression of miR-21 evident in the KYSE-150 cells (Figure 3C). Thus, the KYSE-150 cells were selected for subsequent experimentation.

Next, in an attempt to elucidate the regulatory role of miR-21 and SPRY1 in ESCC cells, miR-21 agomir or miR-21 antagomir and their corresponding NC lentiviruses were transduced into KYSE-150 cells, and adopted RT-qPCR and immunoblotting to evaluate the expression of SPRY1. The results of which indicated that the mRNA and protein expression pattern of SPRY1 was markedly diminished in cells infected with the miR-21 agomir compared to the agomir-NC, while a contradictory trend was identified in the cells infected with the miR-21 antagomir

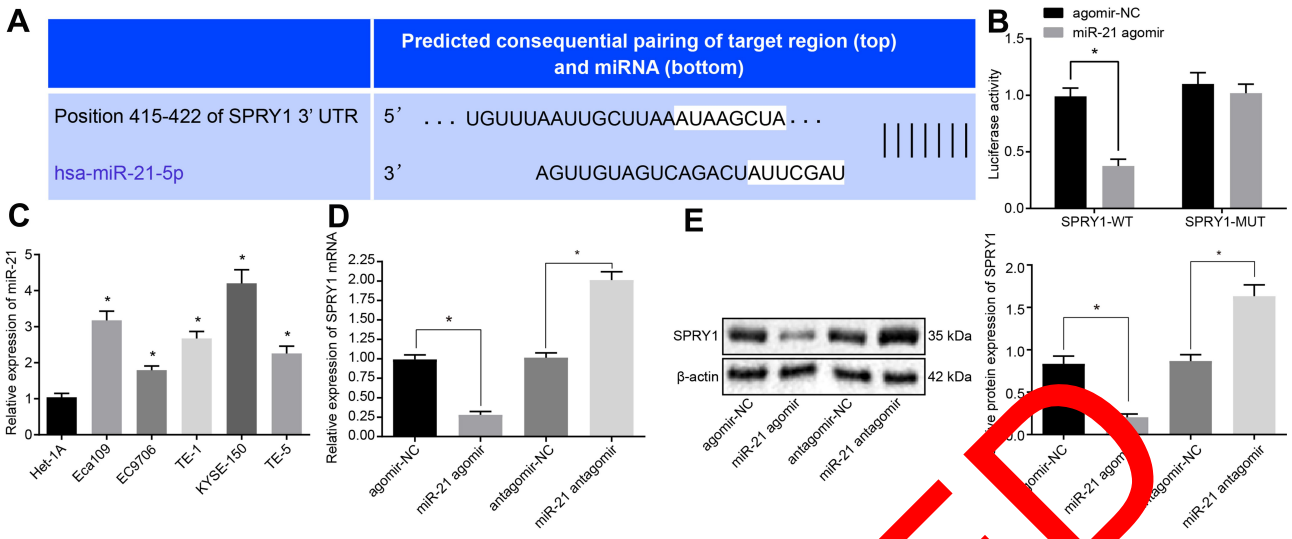

Figure 3 MiR-21 targets and inversely regulates SPRY1. The lentiviruses containing miR-21 agomir, miR-21 antagomir or the corresponding NCs were infected into the cells. (**A**) The specific binding site between SPRY1 and miR-21 predicted by online analysis. (**B**) The binding of miR-21 to SPRY1 3′UTR confirmed by dual luciferase reporter assay. (**C**) The expression pattern of miR-21 in the human normal esophageal epithelial cell line (Het-1A) and human ESCC cell lines (EC9706, Eca109, KYSE-150, TE-1, and TE-5) determined using RT-qPCR. (**D**) The mRNA expression pattern of SPRY1 determined using RT-qPCR. (**E**) The protein expression pattern of SPRY1 determined using immunoblotting. *$p < 0.05$ *vs* cells treated with agomir-NC. Unpaired *t*-test was adopted for data comparison between two groups. Comparisons among multiple groups were conducted by one-way ANOVA, followed by a Tukey's post hoc test. The experiment was conducted three times independently.

compared to the antagomir-NC ($p < 0.05$) (Figure 3D and E). An analysis of the expression patterns of miR-21 and SPRY1 and the clinicopathological characteristics of ESCC (Table 3) revealed that the expression patterns of miR-21 and SPRY1 were correlated with the TNM stage and tissue differentiation of patients with ESCC, but not with their age and gender. Altogether, our results suggested that miR-21 could target SPRY1 and adversely regulate its expression.

Identification of Exosomes Derived from ESCC Cells

KYSE-150-derived exosomes were subjected to TEM. As depicted in Figure 4A, the exosomes were solid and dense

Table 3 Expression of miR-21 and SPRY1 and Clinicopathological Features of ESCC

Clinicopathological Parameters	Cases	miR-21 Expression			SPRY1 Expression		
		High	Low	*p*	High	Low	*p*
Gender				>0.05			>0.05
Male	85	41	44		43	42	
Female	28	16	12		14	14	
Age (year)				>0.05			>0.05
≥61	64	34	30		32	32	
<61	49	23	26		25	24	
Degree of tissue differentiation				<0.05			<0.05
Low	27	21	6		8	19	
Moderate	53	26	27		26	27	
High	33	10	23		23	10	
TNM staging				<0.05			<0.05
I	11	1	10		7	4	
II	50	7	43		40	10	
III	52	49	3		10	42	

Notes: The counting data were analyzed by chi square test.

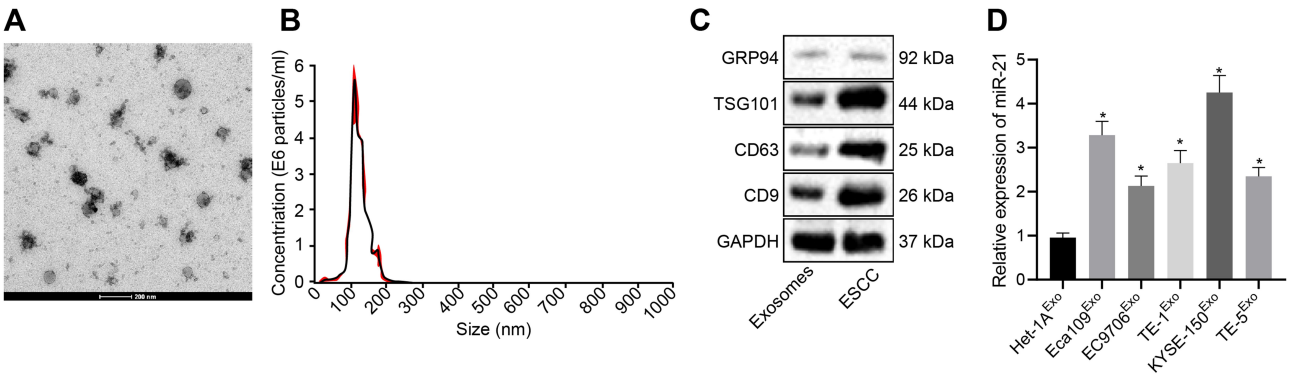

Figure 4 KYSE-150 cells secrete exosomes. (**A**) The morphological observation of exosomes under TEM (scale bar = 200 nm). (**B**) Nanoparticle tracking analysis of exosomes. (**C**) The protein expression pattern of exosome markers CD9, CD63, TSG101, and GRP94 as detected by Western blot analysis (GRP94: 92 kDa, TSG101: 44 kDa, CD9: 25 kDa, CD63: 26 kDa). (**D**) Expression pattern of miR-21 in the exosomes of ESCC cells as determined using RT-qPCR. $^{*}p < 0.05$ vs Het-1A cells.

with a cup- and spherical shaped appearance with diameters ranging from 30 to 180 nm upon visualization under a TEM. Nanoparticle tracking analysis revealed that the size of these exosomes was primarily ranged between 30–200 nm (Figure 4B). Western blot analysis demonstrated that the protein levels of the exosome markers CD9, CD63, and TSG101 were highly expressed, while GRP94 was poorly expressed in the exosomes (Figure 4C). The aforementioned findings were largely indicative of successful isolation of exosomes.

Meanwhile, RT-qPCR (Figure 4D) revealed an increase in the miR-21 expression pattern in exosomes from Eca109, EC9706, Eca109, EC9706, TE-1 and KYSE-150 cells compared with the exosomes in Het-1A cells with the highest expression pattern of miR-21 evident in exosomes of KYSE-150 cells ($p < 0.05$).

ESCC Cell-Secreted Exosomes Transport miR-21 to HUVECs

Next, to ascertain whether ESCC cell-derived exosomes could transport miR-21 to HUVECs, we adopted RT-qPCR (Figure 5A) to evaluate the expression pattern of miR-21 in KYSE-150 cell-derived exosomes. The obtained results revealed a potent rise in the expression pattern of miR-21 in KYSE-150 cells infected with miR-21 agomir compared to control ($p < 0.05$). As shown in Figure 5B, RT-qPCR was employed to assess the expression pattern of miR-21 after co-culture of exosomes and HUVECs, which revealed no discernible difference in the miR-21 expression pattern in KYSE-150 cell-derived exosomes infected with agomir-NC ($p > 0.05$), while a considerable rise in the expression pattern of miR-21 was observed in KYSE-150 cell-derived exosomes infected with the miR-21 agomir in comparison to the control ($p < 0.05$). Exosomes were then labeled with Exo-Red and the fluorescence microscope was employed to observe the uptake of fluorescent-labeled exosomes by HUVECs, the results of which (Figure 5C) demonstrated that the nucleus was stained blue with a substantial amount of red particles in the cytoplasm, corresponding to the uptake of exosomes by HUVECs. Collectively, ESCC cell-derived miR-21 could be transported to HUVECs.

Exosome-Encapsulated miR-21 Released from ESCC Cells Downregulates SPRY1 and Promotes HUVEC Proliferation and Angiogenesis via VEGF Elevation

To further elucidate the underlying mechanism of miR-21 on ESCC cells, ELISA was performed to determine the expression pattern of VEGF following co-culture of exosomes and HUVECs, which revealed no apparent difference in the VEGF expression pattern in KYSE-150 cell-derived exosomes infected with the agomir-NC ($p > 0.05$), while a marked rise in the VEGF expression pattern was evident in KYSE-150 cell-derived exosomes infected with miR-21 agomir compared to the normal control; however, these findings were abrogated by subsequent treatment with oe-SPRY1 ($p < 0.05$) (Figure 6A), suggesting that exosome-encapsulated miR-21 could positively regulate the expression pattern of VEGF, where SPRY1 elevation could inhibit the VEGF expression pattern.

RT-qPCR was performed to ascertain the mRNA expression pattern of SPRY1 following the co-culture of exosomes and HUVECs. No significant difference was evident in terms of SPRY1 mRNA expression pattern in KYSE-150 cell-derived exosomes infected with the agomir-NC ($p > 0.05$), but a marked reduction in SPRY1

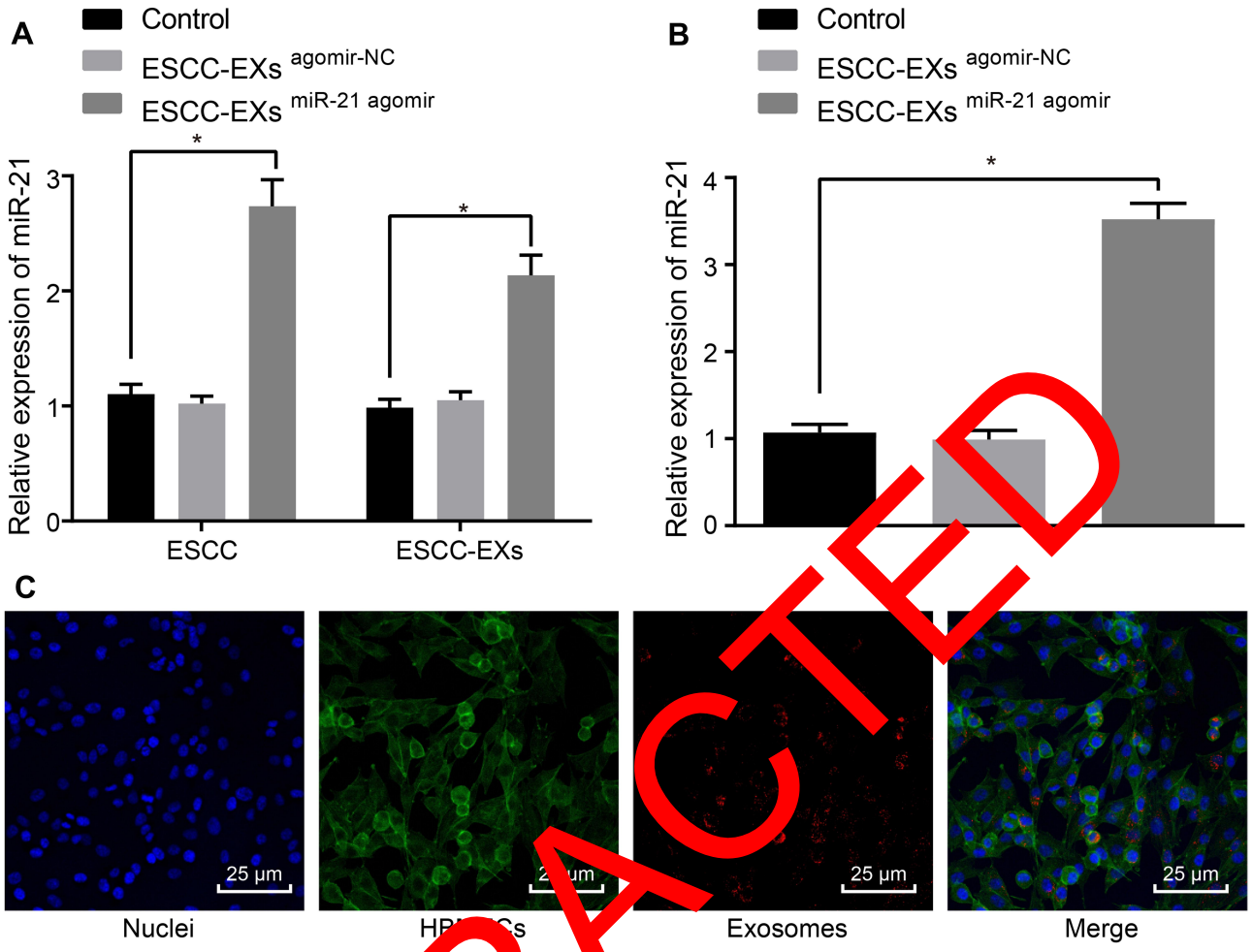

Figure 5 ESCC cell-released exosomes transport miR-21 to HUVECs. (**A**) The expression pattern of miR-21 in the ESCC cells and exosomes assessed using RT-qPCR. (**B**) The expression pattern of miR-21 after co-culture of exosomes and HUVECs assessed using RT-qPCR. (**C**) The uptake of fluorescent-labeled exosomes by HUVECs assessed under the fluorescence microscope. PKH26-labeled exosomes (red), HUVECs (green), DAPI nuclear (blue). *$p < 0.05$ *vs* controls. Comparisons among multiple groups were conducted by one-way ANOVA followed by the Tukey's post hoc test. The experiment was conducted three times independently.

mRNA expression pattern was apparent in the KYSE-150 cell-derived exosomes infected with the miR-21 agomir compared to the control, whereas the effects on miR-21 agomir on the SPRY1 expression pattern were reversed by treatment with oe-SPRY1 ($p < 0.05$) (Figure 6B), indicating that exosome-encapsulated miR-21 could inversely regulate the mRNA expression pattern of SPRY1.

The proliferation of the HUVECs was assessed using CCK-8 as depicted in Figure 6C, which revealed elevated proliferation of HUVECs over time, in addition to markedly elevated HUVEC proliferation in ESCC cell-derived exosomes infected with the miR-21 agomir compared to infection with agomir-NC or control, while further treatment with oe-SPRY1 reduced the proliferation of HUVECs ($p < 0.05$). Colony formation assay and microtubule formation in vitro results (Figure 6D-G) revealed a notable increase in the formation of colonies and tube formation in the KYSE-150 cell-derived exosomes infected with the miR-21 agomir compared to normal control ($p < 0.05$); however, no obvious change was evident in the formed colonies and tube formation in ESCC cell-derived exosomes infected with agomir-NC, while these findings were annulled trend by subsequent treatment with oe-SPRY1 ($p > 0.05$). Altogether, the aforementioned results suggested that the exosome-encapsulated miR-21 promoted HUVEC proliferation and angiogenesis.

The expression pattern of VEGF in the HUVECs was subsequently detected by means of RT-qPCR and immunoblotting (Figure 6H-J), which identified a marked rise in the VEGF mRNA and protein expression pattern in ESCC cell-derived exosomes infected with miR-21 agomir compared to control ($p < 0.05$), while no significant difference was identified corresponding to the VEGF expression in ESCC cell-derived exosomes infected with agomir-NC

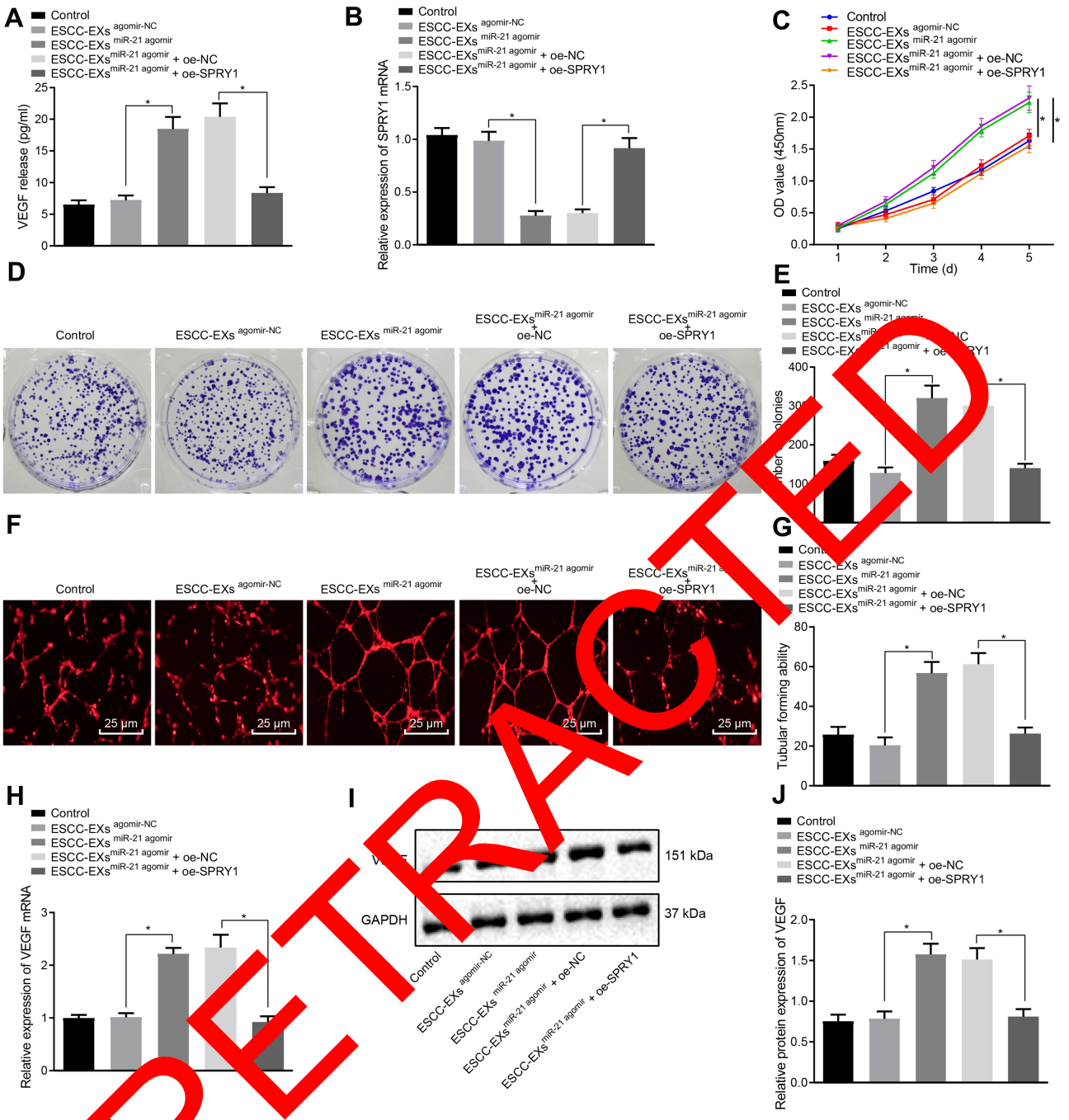

Figure 6 Exosome-encapsulated miR-21 released from ESCC cells represses SPRY1 and expedites HUVEC proliferation and angiogenesis via VEGF upregulation. ESCC cells were infected with the miR-21 agomir, agomir-NC, control, miR-21 agomir + oe-SPRY1 or miR-21 agomir + oe-NC. (**A**) The expression pattern of VEGF after co-culture of exosomes and HUVECs as determined by ELISA. (**B**) The mRNA expression pattern of SPRY1 following the co-culture of exosomes and HUVECs as measured using RT-qPCR. (**C**) The proliferation of HUVECs assessed using CCK-8. (**D, E**) Colony formation ability of HUVECs assessed using colony formation assay. (**F**) Tube formation of HUVECs assessed using tubular formation assay observed under an inverted microscope (scale bars = 25 μm). (**G**) Tube formation of HUVECs assessed using tubular formation assay (VEGF: 151 kDa). (**H**) The mRNA expression pattern of VEGF in HUVECs as assessed by RT-qPCR. (**I, J**) The protein expression pattern of VEGF in HUVECs as assessed by immunoblotting. *$p < 0.05$ *vs* controls. Comparisons among multiple groups were conducted by one-way ANOVA, followed by the Tukey's post hoc test (**A, B, E, G, H**, and (**J**). Statistical analysis in relation to time-based measurements within each group was realized using repeated measures ANOVA, followed by the Bonferroni's post hoc test (**C**). The experiment was conducted three times independently.

($p > 0.05$), while a considerable reduction in the VEGF expression pattern was apparent in ESCC cell-derived exosomes infected with miR-21 agomir and oe-SPRY1 compared to those treated with oe-NC, thereby suggesting that exosome-encapsulated miR-21 could positively regulate the expression of VEGF.

Articulately, exosome-encapsulated miR-21 repressed SPRY1 and promoted HUVEC proliferation and

angiogenesis via VEGF elevation, which was reversed by SPRY1 overexpression.

Elevation of miR-21 Contributes to the Angiogenesis by Repressing SPRY1 and Increasing VEGF Expression in vivo

To further ascertain the regulatory role of miR-21 in ECSS, CAM models were established, after which the number of branching of blood vessels embedded in Matrigel in the surrounding 5 mm area after 10-d incubation was determined. The results revealed a higher proportion of branching of blood vessels in response to miR-21 agomir compared to agomir-NC, while contradictory findings were observed in response to miR-21 antagomir compared to the antagomir-NC ($p < 0.05$) (Figure 7A and B), suggesting that the overexpression of miR-21 contributed to the angiogenesis of the CAM models.

All nude mice xenografted with the KYSE-150 cells exhibited tumor formation. After 2–4 weeks of modeling, the upper abdomen of the nude mice developed a bulge with a hard tumor mass. The nude mice were evidently weaker and anorexic with signs of mental fatigue and stiff limbs. Thereafter, we isolated mouse serum exosomes, RT-qPCR (Figure 7C) showed that the CAM models injected with ESCCs infected with miR-21 agomir potently increased the miR-21 level in the serum exosomes compared with agomir-NC, while conflicting findings were observed in response to the miR-21 antagomir compared with the antagomir-NC. All tumor tissues were confirmed by pathological diagnosis, and the results (Figure 7D-F) showed increased volume and weight of tumor in mice injected with the miR-21 agomir compared to the agomir-NC, while a contrasting trend was observed in response to miR-21 antagomir compared to the antagomir-NC ($p < 0.05$).

The MVD evaluation results (Figure 7G and H) revealed that the cells were stained brown or tan color in the blood vessels. The miR-21 agomir-injected mice exhibited increased MVD compared to the mice injected with agomir-NC, while reduced MVD was detected in response to miR-21 antagomir compared to the antagomir-NC ($p < 0.05$), suggesting that the miR-21 overexpression contributed to the angiogenesis in nude mice xenografted with the KYSE-150 cells.

Finally, immunoblotting was conducted to determine the protein expression patterns of VEGF and SPRY1 in

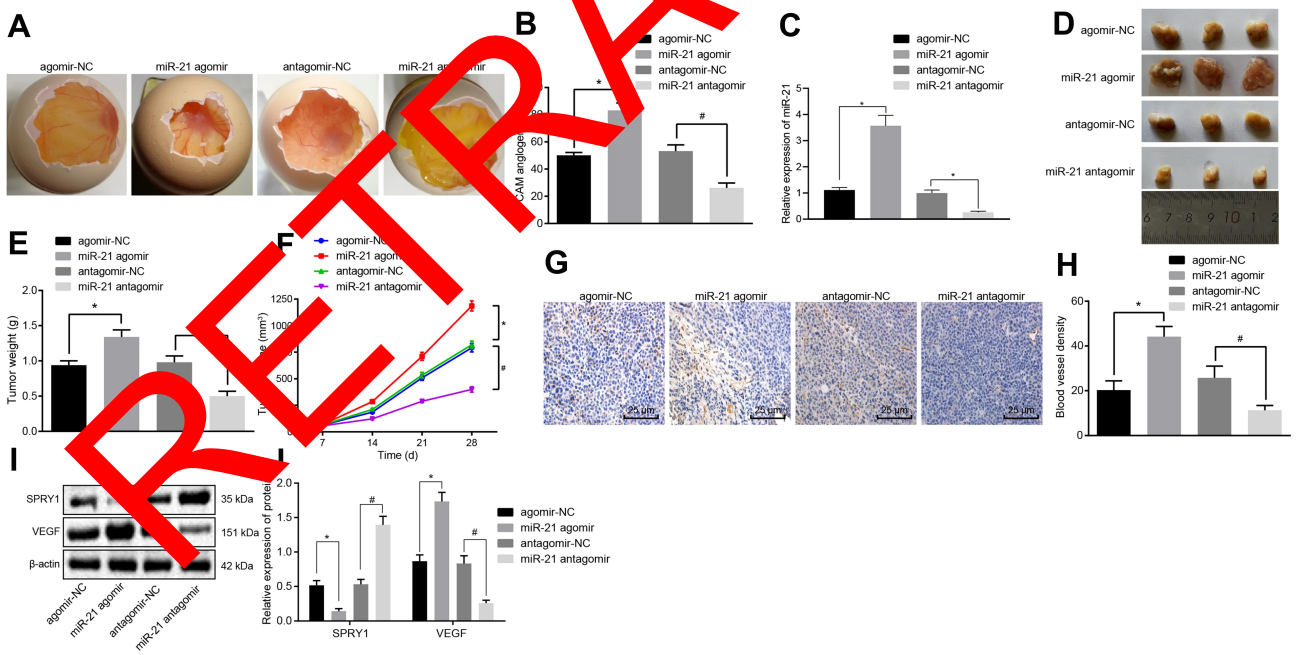

Figure 7 The elevation of miR-21 promotes the angiogenesis in vivo. CAM model and nude mice were transduced with the miR-21 agomir, agomir-NC, miR-21 antagomir or antagomir-NC. (**A**) The angiogenesis observed in CAM model (scale bar = 2 mm; n = 8). (**B**) The branching of blood vessels embedded in Matrigel in the surrounding 5 mm area counted after 10-d incubation in CAM model (n = 10). (**C**) The expression pattern of miR-21 in the serum of CAM model as determined using RT-qPCR. (**D–F**) The formation, volume, and weight of tumor in nude mice xenografted with KYSE-150 cells (n = 8). (**G**) MVD evaluation of mice tumor tissues (scale bar = 25 μm; n = 8). (**H**) MVD evaluation of mice tumor tissues (n = 8). (**I, J**) The protein expression patterns of SPRY1 and VEGF determined using immunoblotting (SPRY1: 35 kDa, VEGF: 151 kDa) (n = 8). *$p < 0.05$ *vs* treatment with agomir-NC, #$p < 0.05$ *vs* treatment with antagomir-NC. Comparisons among multiple groups were conducted by one-way ANOVA, followed by a Tukey's post hoc test. Statistical analysis in relation to time-based measurements within each group was realized using repeated measures ANOVA, followed by a Bonferroni's post hoc test (**E**).

mice tumor tissues. The results revealed that the VEGF expression pattern was upregulated, while the SPRY1 expression pattern was downregulated in response to miR-21 agomir compared to the agomir-NC, with an opposite trend evident in response to miR-21 antagomir compared to the antagomir-NC ($p < 0.05$) (Figure 7I and J), suggesting that miR-21 inhibited the SPRY1 expression pattern, while amplifying the VEGF expression pattern. These findings supported the notion that miR-21 overexpression contributes to angiogenesis in vivo via SPRY1 inhibition and VEGF elevation.

Discussion

The diagnosis of ESCC is frequently manifested with poor prognosis, largely attributable to the diagnosis at an advanced stage. The principal causative ESCC factors exhibit considerable variations across the globe, thereby complicating the analysis of its epidemiology.[32] Abnormal angiogenesis has been proposed to significantly influence the cancer progression, from the proliferation, migration, lumen formation, and differentiation to maturation of definite endothelial cell functions.[33] In the current study, we investigated the underlying mechanism associated with exosome-encapsulated miR-21 secreted from ESCC cells in regard with the angiogenesis of HUVECs in ESCC. Our findings suggested that the transfer of miR-21 from ESCC cell-derived exosomes could potentially downregulate SPRY1, and ultimately stimulate the angiogenesis of HUVECs via VEGF upregulation.

Our initial findings revealed that the expression of miR-21 was upregulated in ESCC tissues and cells, and its upregulation subsequently stimulated the proliferation and angiogenesis in HUVECs. In consistency with our findings, an existing study identified elevated miR-21 expressions in the serum samples from ESCC patients, thereby suggesting a positive correlation between miR-21 and the progression of ESCC.[17] Additionally, downregulation of the miR-21 expression has been implicated in the event of inhibited proliferation and enhanced apoptosis of ESCC cells.[34] Meanwhile, miR-21 has demonstrated its simulative effect on tumor angiogenesis by targeting PTEN to activate the AKT and ERK1/2 signaling pathways, thereby enhancing the HIF-1α and VEGF expression.[35] Correspondingly, an existing study elicited the ability of overexpression of miR-21 to potentially facilitate retinal vascular endothelial cell viability and angiogenesis in rats with diabetic retinopathy via activation of the PI3K/AKT/VEGF signaling pathway and repression of the PTEN expression.[36] Recent years have witnessed significant advancements regarding investigation of exosome-mediated transport of non-coding RNAs (ncRNA) between stem cells and cancer cells, whereby exosome-ncRNAs have demonstrated functionality as mediators, imparting a bystander effect on the secreting cancer stem cells into recipient cells for priming a tumor permissive environment and eliciting therapeutic resistance.[37] Exosome-derived miR-21 from the transformed human bronchial epithelial cells was reported to stimulate the angiogenesis in HUVECs, while its repression could evidently annul the stimulatory effect on angiogenesis in lung cancer.[18] In addition, the in vivo experiments further verified our findings demonstrating that miR-21 downregulation inhibits the angiogenesis of HUVECs which was evidenced by a reduction in the number of branches of microvessels in CAM and decreased MVD in nude mice xenografted with ESCC cells. An elevated number of branches of microvessels have been reported to serve as an indicator of tumor angiogenesis in CAM,[35] while an increase in MVD serves as an indicator of angiogenesis.[38] The aforementioned findings supported the notion that the delivery of miR-21 from ESCC cell-derived exosomes fundamentally stimulated HUVEC proliferation and angiogenesis.

Our findings from subsequent experimentation demonstrated that the expression of SPRY1 was downregulated in ESCC tissues and cells, while its elevation by exosome-derived miR-21 hindered the proliferation and angiogenesis in HUVECs. The regulatory role of miR-21 in SPRY1 has been previously investigated in glioma, where the knockdown of SPRY1 contributed in facilitating the proliferation and inhibiting the apoptosis of glioma cells.[39] Interestingly, SPRY1 has coherently emerged as an endogenous inhibitor for angiogenesis, while the depletion of SPRY1 could radically impair apoptosis and trigger migration along with tube formation of endothelial cells.[40] Downregulation of the SPRY1 gene by miR-21 overexpression improves activity of the VEGF expression, a process that can be annulled by the miR-21 antagomir in ARPE-19 cells.[41] The upregulation of SPRY1 has been demonstrated to inhibit VEGF-induced endothelial cell proliferation.[42] Additionally, the overexpression of SPRY1 could fundamentally prevent VEGF secretion, a vital element for primary tumor growth, migration, and invasion in human breast cancer cells.[43]

VEGF has been extensively documented as a secreted mitogen associated with angiogenesis, which can also

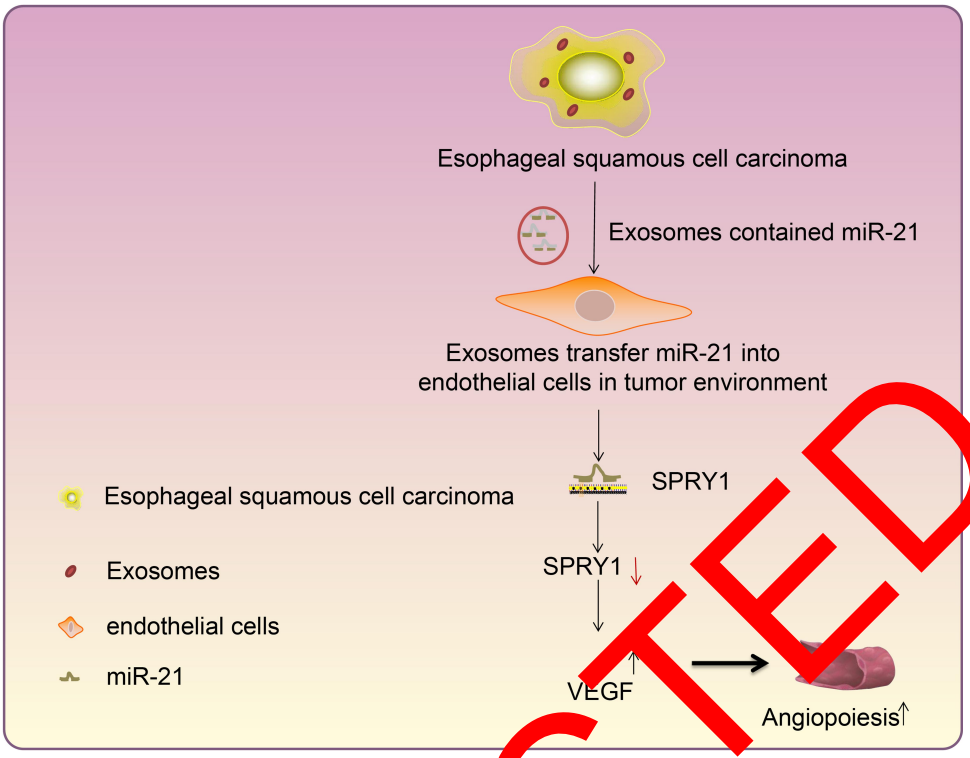

Figure 8 Mechanistic investigations indicate exosome-encapsulated miR-21 release from ESCC cells downregulates the SPRY1 expression and promotes HUVEC proliferation and angiogenesis via VEGF elevation, thereby exacerbating ESCC.

serve as a potent vascular permeability factor.[44] Our results demonstrated that the VEGF expression was elevated in ESCC tissues, and its downregulation, positively regulated by miR-21 impairs the proliferation and angiogenesis in HUVECs. Consistently, VEGF has been previously reported to be elevated in cervical ESCC tissues with HPV infection, with existing studies eliciting a positive correlation between VEGF and miR-21.[45] Glioma stem cell-derived exosomes have been reported to stimulate the angiogenic ability of endothelial cells by activation of the miR-21/VEGF/VEGFR2 signal pathway.[46] The depletion of VEGF was employed for superior clinical outcomes of ESCC during concurrent chemoradiotherapy.[47] VEGF along with its family factors is documented as the central components of abnormal angiogenesis with extensive functionality in a wide variety of tumors and diseases.[22] Mechanically, solid tumors by producing VEGF supply the oxygen and essential nutrients for angiogenesis by producing VEGF, thus making the inhibition of VEGF signaling capable of impairing tumor angiogenesis, to consequently suppress tumor growth and metastasis.[48] An existing study concluded that the conditioned media from irradiated MCF-7 cells could induce angiogenic responses in HUVECs in vitro, which may be synchronous with the transfer of increased VEGF-A and perhaps other factors secreted from irradiated MCF-7 cells to HUVECs.[49] Based on the aforementioned literature, we believe that the inhibition of VEGF is a promising anti-angiogenic therapy in ESCC.

Conclusion

In conclusion, the finding of the current study ascertained that exosome-encapsulated miR-21 derived from ESCC cells could be delivered to HUVECs, and subsequently down-regulate the expression pattern of SPRY1 while upregulating the expression pattern of VEGF, ultimately stimulating the proliferation and angiogenesis of HUVECs in ESCC (Figure 8). The findings of the current study highlight the potential of miR-21 as a therapeutic target for ESCC. However, the exact molecular mechanism of miR-21 in ESCC still requires extensive elucidation in a more detailed study encompassing different cell lines. In addition, we only adopted a single dose of exosomes in our experiments. Further studies are necessitated to identify the optimum dose and the number of injections, to confirm the optimal clinical application of miR-21 in ESCC.

Abbreviations

ESCC, esophageal squamous cell carcinoma; miR, microRNA; HUVECs, human umbilical venous endothelial cells; CAM, chicken chorioallantoic membrane; MVD, microvascular density; SPRY1, sprouty RTK signaling antagonist 1; MAPK, Ras-mitogen-activated protein kinase; signaling pathway; VEGF, vascular endothelial growth factor; GEO, Gene Expression Omnibus; DEGs, differentially expressed genes; ATCC, American Type Culture Collection; STR, short-tandem-repeat; RPMI, Roswell Park Memorial Institute; FBS, fetal bovine serum; TNM, tumor node metastasis; AJCC, American Joint Committee on Cancer; DAB, diaminobenzidine; TEM, transmission electron microscope; SDS-PAGE, sodium dodecyl sulfate polyacrylamide gel electrophoresis; TSG101, tumor susceptibility gene 101; BCA, bicinchoninic acid; RT-qPCR, reverse transcription quantitative polymerase chain reaction; WT, wild type; MUT, mutant; ELISA, enzyme-linked immunosorbent assay; OD, optical density; CCK-8, Cell counting kit-8; IgG, immunoglobulin G; TBST, tris-buffered saline Tween-20; NC; ANOVA, analysis of variance.

Acknowledgments

We would like to acknowledge the reviewers for the helpful comments on this paper.

Funding

There is no funding to report.

Disclosure

The authors declare that they have no conflicts of interest for this work.

Reference

1. Bray F, Ferlay J, Soerjomataram I, et al. Global cancer statistics 2018: GLOBOCAN estimates of incidence and mortality worldwide for 36 cancers in 185 countries. *CA Cancer J Clin*. 2018;68(6):394–424. doi:10.3322/caac.21492
2. Rustgi AK, El-Serag HB. Esophageal carcinoma. *N Engl J Med*. 2014;371(26):2499–2509. doi:10.1056/NEJMra1314530
3. Siegel RL, Miller KD, Jemal A. Cancer statistics, 2019. *CA Cancer J Clin*. 2019;69(1):7–34. doi:10.3322/caac.21551
4. Murphy G, McCormack V, Abedi-Ardekani B, et al. International cancer seminars: a focus on esophageal squamous cell carcinoma. *Ann Oncol*. 2017;28(9):2086–2093. doi:10.1093/annonc/mdx279
5. Ma Q, Reiter RJ, Chen Y. Role of melatonin in controlling angiogenesis under physiological and pathological conditions. *Angiogenesis*. 2020;23(2):91–104. doi:10.1007/s10456-019-09689-7
6. Jayson GC, Kerbel R, Ellis LM, Harris AL. Antiangiogenic therapy in oncology: current status and future directions. *Lancet*. 2016;388 (10043):518–529. doi:10.1016/S0140-6736(15)01088-0
7. Noma K, Smalley KS, Lioni M, et al. The essential role of fibroblasts in esophageal squamous cell carcinoma-induced angiogenesis. *Gastroenterology*. 2008;134(7):1981–1993. doi:10.1053/j.gastro.2008.02.061
8. Zhang X, Yuan X, Shi H, et al. Exosomes in cancer: small particle, big player. *J Hematol Oncol*. 2015;8(1):(83. doi:10.1186/s13045-015-0181-x
9. Zhang Y, Liu Y, Liu H, Tang WH. Exosomes: biogenesis, biologic function and clinical potential. *Cell Biosci*. 2019;9:(19. doi:10.1186/s13578-019-0282-2
10. Mohammadi S, Yousefi F, Shabaninejad Z, et al. Exosomes and cancer: from oncogenic roles to therapeutic applications. *IUBMB Life*. 2020;72(4):724–748. doi:10.1002/iub.2182
11. Jamali L, Tofigh R, Tutunchi S, et al. Circulating microRNAs as diagnostic and therapeutic biomarkers in gastric and esophageal cancers. *J Cell Physiol*. 2018;233(11):8538–8550. doi:10.1002/jcp.26850
12. He L, Zhu W, Chen Q, et al. Ovarian cancer cell-secreted exosomal miR-205 promotes metastasis by inducing angiogenesis. *Theranostics*. 2019;9(26):8206–8220. doi:10.7150/thno.37455
13. Guo S, Xu X, Ouyang Y, et al. Microarray expression profile analysis of circular RNAs in pancreatic cancer. *Mol Med Rep*. 2018;17 (6):7661–7671. doi:10.3892/mmr.2018.8827
14. Chen F, Chu L, Li et al. Hypoxia induced changes in miRNAs and their target mRNAs in extracellular vesicles of esophageal squamous cancer cells. *Mol Cancer*. 2020;:570–580. doi:10.1111/1759-7714.13295
15. Harrandah AM, Mora , Chan EKL. Emerging microRNAs in cancer diagnosis, progression, and immune surveillance. *Cancer Lett*. 2018;438:(126–132. doi:10.1016/j.canlet.2018.09.019
16. Wei LL, Qiu Y, Zhang B, Shi ZZ. MicroRNAs in esophageal squamous cell carcinoma: potential biomarkers and therapeutic targets. *Cancer Biomark*. 2017;19(1):1–9. doi:10.3233/CBM-160240
17. Tanaka Y, Tamohara H, Kinoshita K, et al. Clinical impact of serum exosomal microRNA-21 as a clinical biomarker in human esophageal squamous cell carcinoma. *Cancer*. 2013;119(6):1159–1167. doi:10.1002/cncr.27895
18. Liu Y, Luo F, Wang B, et al. STAT3-regulated exosomal miR-21 promotes angiogenesis and is involved in neoplastic processes of transformed human bronchial epithelial cells. *Cancer Lett*. 2016;370 (1):125–135. doi:10.1016/j.canlet.2015.10.011
19. McNeill B, Ostojic A, Rayner KJ, Ruel M, Suuronen EJ. Collagen biomaterial stimulates the production of extracellular vesicles containing microRNA-21 and enhances the proangiogenic function of CD34(+) cells. *FASEB J*. 2019;33(3):4166–4177. doi:10.1096/fj.201801332R
20. Liu X, Lan Y, Zhang D, et al. SPRY1 promotes the degradation of uPAR and inhibits uPAR-mediated cell adhesion and proliferation. *Am J Cancer Res*. 2014;4(6):683–697.
21. Lee S, Bui Nguyen TM, Kovalenko D, et al. Sprouty1 inhibits angiogenesis in association with up-regulation of p21 and p27. *Mol Cell Biochem*. 2010;338(1–2):255–261. doi:10.1007/s11010-009-0359-z
22. Wang Q, Li T, Wu Z, et al. Novel VEGF decoy receptor fusion protein conbercept targeting multiple VEGF isoforms provide remarkable anti-angiogenesis effect in vivo. *PLoS One*. 2013;8(8): e70544. doi:10.1371/journal.pone.0070544
23. Potente M, Gerhardt H, Carmeliet P. Basic and therapeutic aspects of angiogenesis. *Cell*. 2011;146(6):873–887. doi:10.1016/j.cell.2011.08.039
24. Li CH, Sun XJ, Niu SS, et al. Overexpression of IQGAP1 promotes the angiogenesis of esophageal squamous cell carcinoma through the AKT and ERKmediated VEGFVEGFR2 signaling pathway. *Oncol Rep*. 2018;40(3):1795–1802. doi:10.3892/or.2018.6558
25. Demerdash HM, Hussien HM, Hassouna E, Arida EA. Detection of MicroRNA in hepatic cirrhosis and hepatocellular carcinoma in hepatitis C genotype-4 in Egyptian patients. *Biomed Res Int*. 2017;2017:(1806069. doi:10.1155/2017/1806069

26. Hsu PK, Chen HS, Liu CC, Wu SC. Application of the eighth AJCC TNM staging system in patients with esophageal squamous cell carcinoma. *Ann Thorac Surg*. 2018;105(5):1516–1522. doi:10.1016/j.athoracsur.2017.12.032
27. Xiaoyu H, Yiru Y, Shuisheng S, et al. The mTOR pathway regulates PKM2 to affect glycolysis in esophageal squamous cell carcinoma. *Technol Cancer Res Treat*. 2018;17:(1533033818780063. doi:10.1177/1533033818780063
28. Wang XC, Zhang ZB, Wang YY, et al. Increased miRNA-22 expression sensitizes esophageal squamous cell carcinoma to irradiation. *J Radiat Res*. 2013;54(3):401–408. doi:10.1093/jrr/rrs113
29. Essone J, N'Dilimabaka N, Ondzaga J, et al. Comparison of apoptosis in human primary pulmonary endothelial cells and a brain microvascular endothelial cell line co-cultured with plasmodium falciparum field isolates. *BMC Infect Dis*. 2017;17(1):454. doi:10.1186/s12879-017-2552-0
30. Weidner N, Folkman J, Pozza F, et al. Tumor angiogenesis: a new significant and independent prognostic indicator in early-stage breast carcinoma. *J Natl Cancer Inst*. 1992;84(24):1875–1887. doi:10.1093/jnci/84.24.1875
31. Zhou Y, Zhu Y, Zhang L, et al. Human stem cells overexpressing miR-21 promote angiogenesis in critical limb ischemia by targeting CHIP to enhance HIF-1alpha activity. *Stem Cells*. 2016;34(4):924–934. doi:10.1002/stem.2321
32. Abnet CC, Arnold M, Wei WQ. Epidemiology of esophageal squamous cell carcinoma. *Gastroenterology*. 2018;154(2):360–373. doi:10.1053/j.gastro.2017.08.023
33. Sajib S, Zahra FT, Lionakis MS, German NA, Mikelis CM. Mechanisms of angiogenesis in microbe-regulated inflammatory and neoplastic conditions. *Angiogenesis*. 2018;21(1):1–14. doi:10.1007/s10456-017-9583-4
34. Li X, Chen D, Li M, et al. The CADM2/Akt pathway is involved in the inhibitory effect of miR-21-5p downregulation on prol[illegible]ion and apoptosis in esophageal squamous cell carcinoma cells. *Chem Biol Interact*. 2018;288:(76–82. doi:10.1016/j.cbi.2018.04.021
35. Liu LZ, Li C, Chen Q, et al. MiR-21 induced angi[illegible]esis thr[illegible] AKT and ERK activation and HIF-1alpha ex[illegible]ssion. *PLoS O[illegible]* 2011;6(4):e19139. doi:10.1371/journal.pone.[illegible]19139
36. Lu JM, Zhang ZZ, Ma X, Fang SF, [illegible] XH. [illegible]ion o[illegible] microRNA-21 inhibits retinal vascula[illegible]endoth[illegible]ell growth and angiogenesis via PTEN dependent [illegible]3K/Akt/VE[illegible] signaling pathway in diabetic retinopathy. [illegible]*Eye Res*. 20[illegible]190:(107886. doi:10.1016/j.exer.2019.10788[illegible]
37. Nawaz M. Extracellular [illegible]sicle-mediate[illegible]ransport of non-coding RNAs between stem [illegible]s and cancer cells: [illegible]plications in tumor progression and the[illegible]peutic res[illegible]tance. *Stem Cell Investig*. 2017;4:(83. doi:10.21037/[illegible]2017.1[illegible]4
38. Lan J, Li J, Ju X, et al. Relationship between microvessel density and cancer stem cells in tumor angiogenesis: a meta-analysis. *Biomark Med*. 2016;10(8):919–932. doi:10.2217/bmm-2016-0026
39. Chai C, Song LJ, Han SY, Li XQ, Li M. MicroRNA-21 promotes glioma cell proliferation and inhibits senescence and apoptosis by targeting SPRY1 via the PTEN/PI3K/AKT signaling pathway. *CNS Neurosci Ther*. 2018;24(5):369–380. doi:10.1111/cns.12785
40. Sabatel C, Cornet AM, Tabruyn SP, et al. Sprouty1, a new target of the angiostatic agent 16K prolactin, negatively regulates angiogenesis. *Mol Cancer*. 2010;9(1):(231. doi:10.1186/1476-4598-9-231
41. Haque R, Iuvone PM, He L, et al. The MicroRNA-21 signaling pathway is involved in prorenin receptor (PRR) -induced VEGF expression in ARPE-19 cells under a hyperglycemic condition. *Mol Vis*. 2017;23:(251–262.
42. Huebert RC, Li Q, Adhikari N, et[illegible] Identifica[illegible]n and regulation of Sprouty1, a negative inhibitor[illegible] the ERK casc[illegible]e, in the human heart. *Physiol Genomics*. 2[illegible]:18(3):284–2[illegible]. doi:10.1152/physiolgenomics.00098.2[illegible]4
43. Mekkawy AH, Pourg[illegible]ami MH, Morri[illegible]DL, [illegible]man Sprouty1 suppresses growth, mi[illegible]tion, and [illegible]vasion in [illegible]man breast cancer cells. *Tumour Biol*. 2014;3[illegible]5):50[illegible]–5048. d[illegible]:10.1007/s13277-014-1665-y
44. Zhang ZG[illegible]hang L, Jiang [illegible]et al. [illegible]EGF enhances angiogenesis and promo[illegible]s blo[illegible]brain barrier [illegible]kage in the ischemic brain. *J Clin Invest*. 2000;106[illegible]829–838. doi:10.1172/JCI9369
45. [illegible]Y, Min SJ, Xu[illegible]Q, et al. Expressions of VEGF and miR-21 in tumor tissues of cervic[illegible] cancer patients with HPV infection and their relationship[illegible]with prognosis. *Eur Rev Med Pharmacol Sci*. 2018;22(19):6274–6[illegible]9. doi:10.26355/eurrev_201810_16035
46. Sun X, Ma[illegible], Wang J, et al. Glioma stem cells-derived exosomes p[illegible]mote[illegible] angiogenic ability of endothelial cells through miR-21/VEGF signal. *Oncotarget*. 2017;8(22):36137–36148. doi:10.18632/[illegible]ncotarget.16661
47. Chen YH, Lu HI, Lo CM, et al. The crucial role of blood VEGF kinetics in patients with locally advanced esophageal squamous cell carcinoma receiving curative concurrent chemoradiotherapy. *BMC Cancer*. 2018;18(1):837. doi:10.1186/s12885-018-4731-9
48. Na HJ, Hwang JY, Lee KS, et al. TRAIL negatively regulates VEGF-induced angiogenesis via caspase-8-mediated enzymatic and non-enzymatic functions. *Angiogenesis*. 2014;17(1):179–194. doi:10.1007/s10456-013-9387-0
49. Jabbari N, Nawaz M, Rezaie J. Bystander effects of ionizing radiation: conditioned media from X-ray irradiated MCF-7 cells increases the angiogenic ability of endothelial cells. *Cell Commun Signal*. 2019;17(1):165. doi:10.1186/s12964-019-0474-8